

Cell Reports, Volume 35

Supplemental information

**Microcircuit mechanisms for the generation
of sharp-wave ripples in the basolateral amygdala:
A role for chandelier interneurons**

Madhusoothanan B. Perumal, Benjamin Latimer, Li Xu, Peter Stratton, Satish Nair, and Pankaj Sah

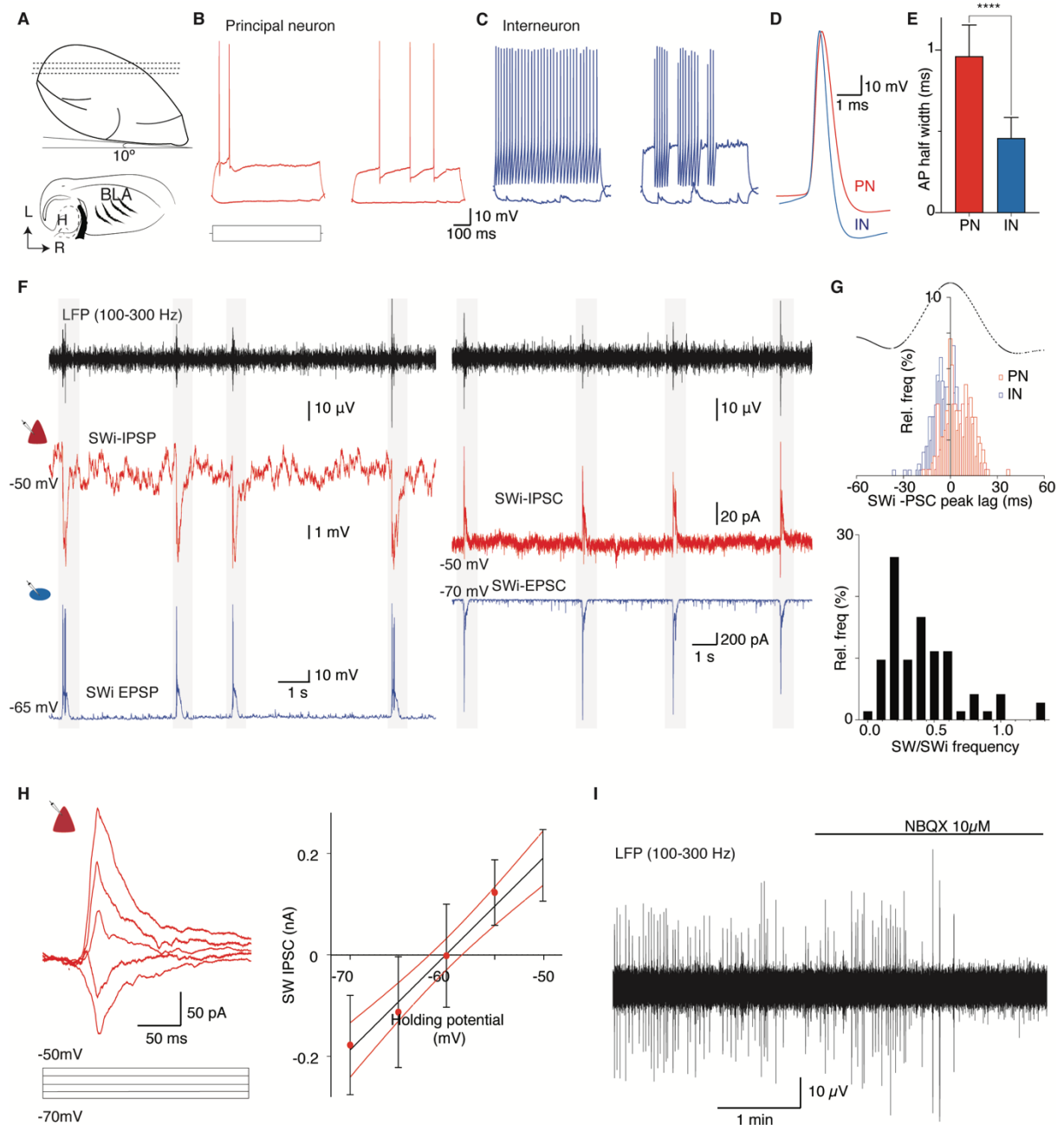


Figure S1. Discharge properties and sharp wave associated intracellular events in principal neurons and interneurons in the basolateral amygdala. Related to Figure 1

(A) Schematic of oblique horizontal slice preparation containing the BLA. Oblique brain slices were prepared with dorsal side of the brain glued to a plate with fronto-occipital angle $\sim 10^\circ$. Bottom, schematic of an oblique horizontal brain slice containing BLA and hippocampus (H). **(B-C)** Depolarizing current injection evoked distinctive action potential (AP) discharge patterns in principal neurons (PNs, red) and interneurons (INs, blue). Traces show two main types of discharge patterns observed in PNs (adaptive and regular) and INs (fast continuous and fast stuttering). **(D)** Superimposed APs recorded in a PN (red) and IN (blue) showing that the PN AP is wider. **(E)** The width at the half-maximal amplitude of AP (AP half-width) in PNs (0.9 ± 2 ms, $n=72$) was significantly wider than in INs (0.4 ± 0.1 ms, $n=54$, t-test with Welch correction, p -value < 0.0001). **(F)** Sharp wave ripple transitions in the local field potential (LFP, black) are correlated with intracellular synaptic events (SWi) in PNs (red) and INs (blue). Traces show the LFP signal filtered for ripple frequency band. Left,

LFP ripples occur with inhibitory post-synaptic potentials (IPSPs) in the PN and excitatory post-synaptic potentials (EPSPs) with a burst of action potentials (AP) in the IN. Right, same pair of cells in voltage clamp showing ripple-associated (grey bars) inhibitory post-synaptic currents (IPSC) in the PN (V_h -50 mV; middle) and excitatory post-synaptic currents (EPSC) in the IN going (V_h -70 mV, bottom). (G) Top, histogram shows lag between peaks of SW and concurrently recorded SW synaptic currents in PNs (red) and INs (blue). Bottom histogram shows frequency of SWs in oblique BLA slices ($n=72$ slices). (H) The peak amplitude of SWi-IPSCs in PNs reversed polarity at the chloride reversal potential ($n=18$). Left, superimposed mean SWi-IPSCs recorded in a PN from -70 mV to -50 mV; right, peak amplitude of SWi-IPSCs (mean \pm SD) plotted against holding potentials (I) Bath application of AMPA receptor antagonist (CNQX or NBQX) abolished SWs in the BLA ($n=3$)

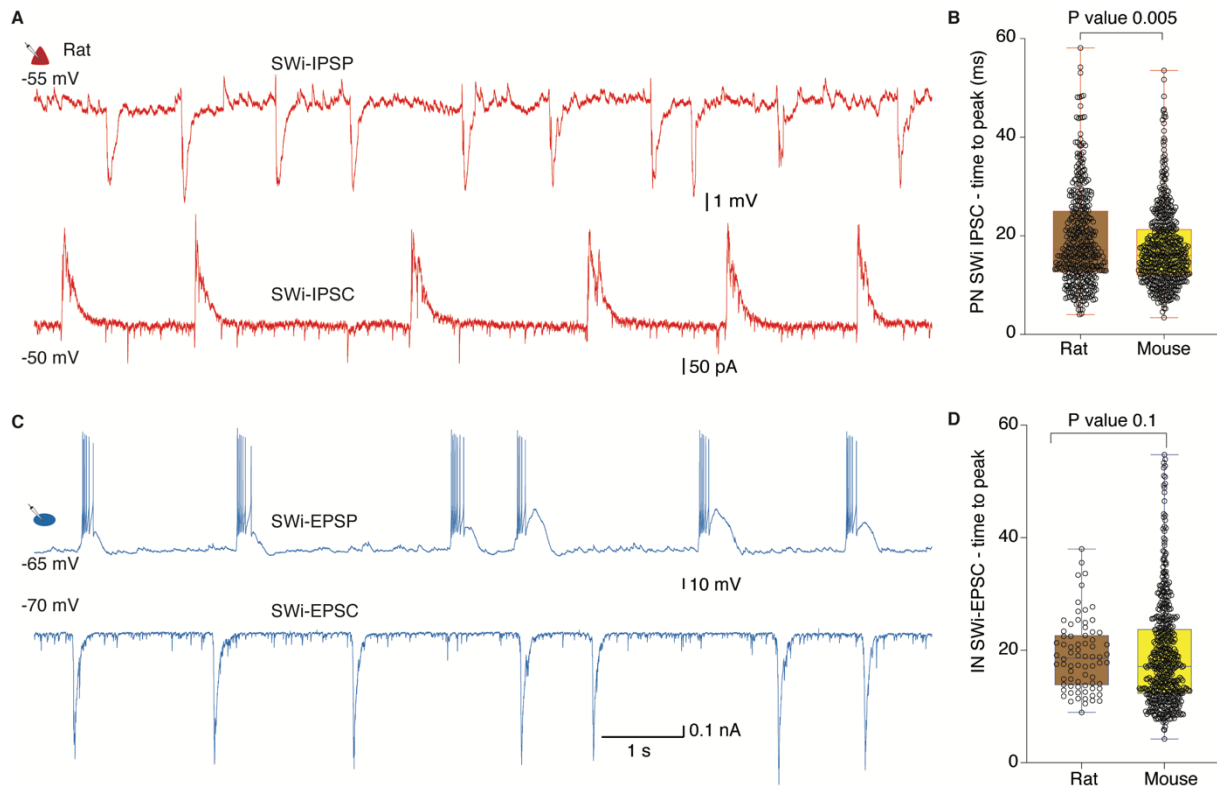


Figure S2. Sharp wave associated synaptic events are similar in rat and mouse. Related to Figure 1

Horizontal slices containing the BLA were prepared from adult rats. **(A)** Top and bottom, whole-cell recording in a PN in a rat BLA slice in current clamp (top) showing SW-associated IPSPs and in voltage clamp showing SW-associated IPSCs (bottom). The time to peak of the synaptic burst of in rats and mice (Figure 1) are shown in the panels in **(B)**. The time to peak in both species are similar (rat, $n=424$ episodes, 19.5 ± 9 ms vs mouse, $n=550$ episodes, 17.6 ± 8 ms, KS test). **(C)** Top and bottom, whole-cell recording in an IN in a rat BLA slice in current clamp (top) showing SW-associated EPSP and a burst of action potentials as in the mouse (Figure 1) and in voltage clamp showing SW-associated EPSCs (bottom). The time to peak of the synaptic burst of in rats and mice (Figure 1) are shown in the panels **(D)** SW-associated EPSCs recorded from rats and mice slices reached peak amplitude in similar time-windows (rat, $n=74$ episodes; mean \pm SD: 19 ± 6 ms vs mice, $n=529$ episodes, mean \pm SD: 19 ± 9 ms, KS test).

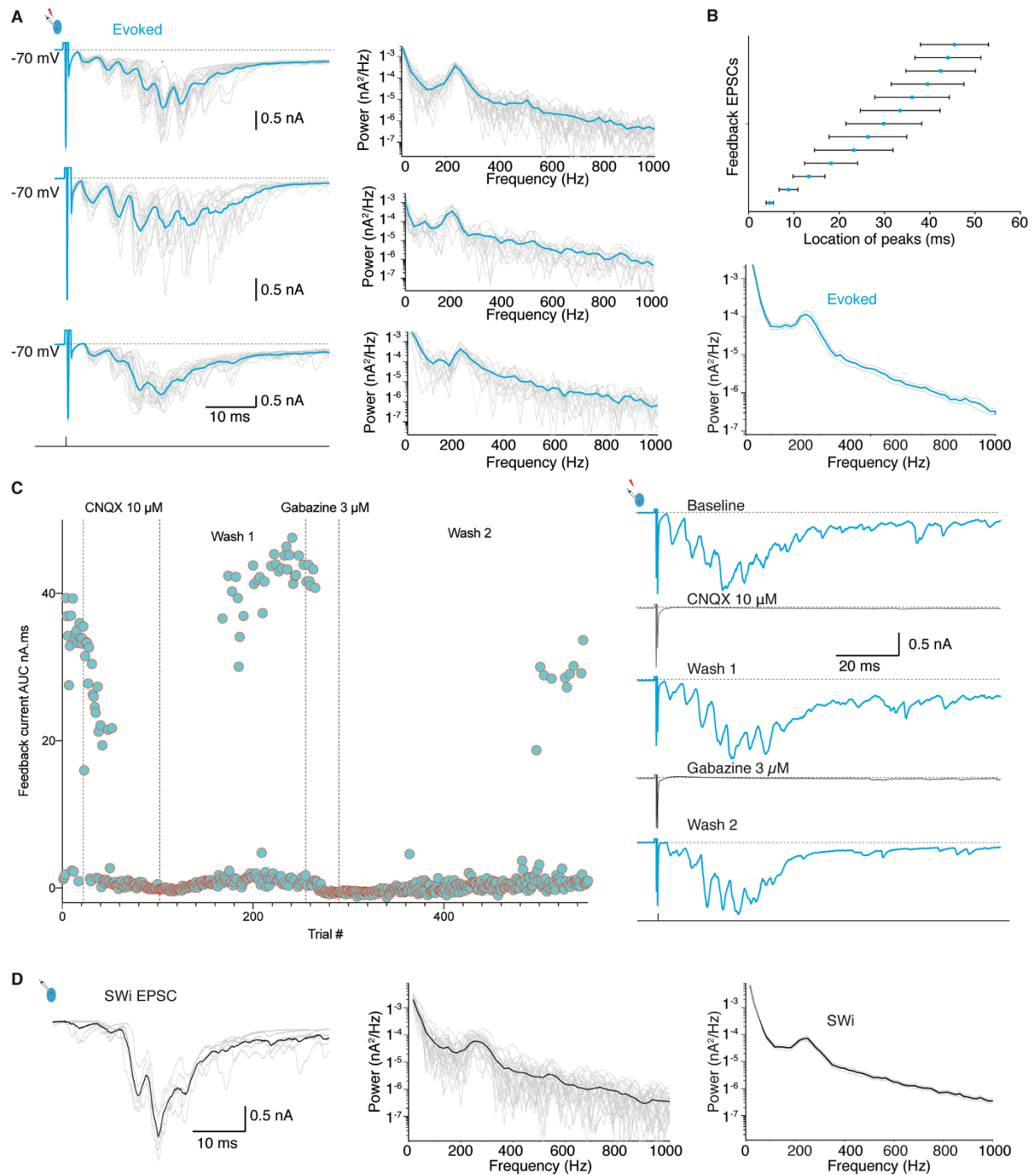


Figure S3. Evoked feedback burst has the same pharmacological sensitivity and temporal structure as the SW-associated intracellular burst (SWi). Related to Figure 2

(A) Whole cell recording from an interneuron (IN). A brief depolarising voltage step (70 mV, 0.5 ms) evokes a stereotypical feedback burst consisting of repetitive EPSCs at time-locked intervals. Left, top to bottom, voltage clamp traces from three INs recorded from 3 different slices. Middle panels show spectral analysis of traces on the left illustrating consistent peak power at ~ 250 Hz; mean spectrum is shown in cyan overlaid on individual trials. (B) Top plot shows timing of successive EPSCs (mean \pm SD) in each feedback bursts of inputs recorded in all cells ($n=468$ trials) revealing time-locked events at ~ 4 ms intervals. Lower plot shows mean ± 2 SEM of spectral analysis of evoked feedback EPSCs ($n=468$ trials) (C) Feedback burst in INs is reversibly blocked by AMPA receptor (CNQX) and GABA_A receptor antagonists (Gabazine). Plot shows AUC of evoked feedback burst sequentially and

reversibly abolished by AMPA and GABA_A receptor antagonists. Representative feedback bursts during the trial are shown on the right (also shown in figure 2 C). **(D)** Representative SW-associated burst of EPSCs showing same temporal structure as IN-evoked feedback burst. Left, voltage clamp recording from an IN showing SW-associated burst of EPSCs; middle, spectral analysis showing peak power at ~250 Hz; right, mean \pm 2SEM of spectral analysis of SW-associated burst EPSCs in the same INs (n=228 episodes); mean in black overlaid on individual episodes.

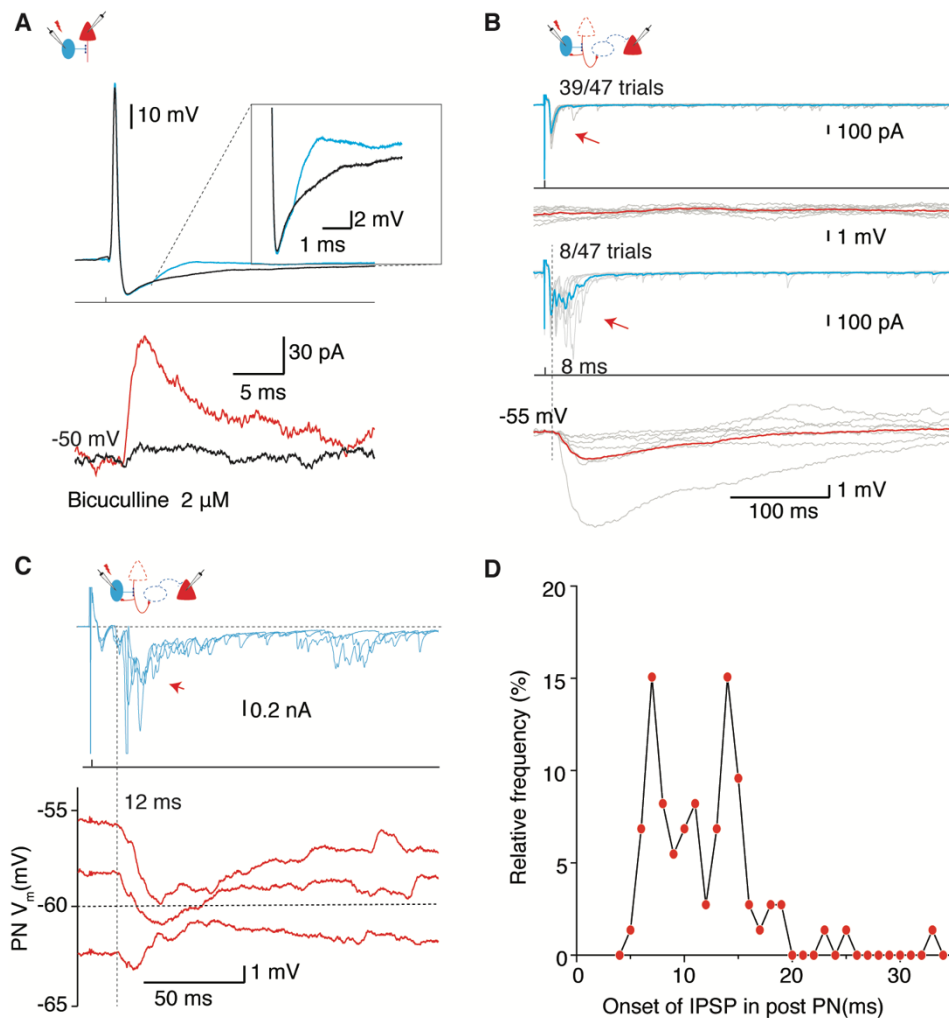


Figure S4 Interneurons with feedback burst excitation evoke network activity and delayed feedforward inhibition in principal neurons. Related to Figure 2.

(A) Paired recording from an IN with feedback-EPSP (top) and a PN (bottom).

Representative traces show the response to depolarizing current injection (2 nA, 0.5 ms) that

evoked an AP in the IN followed by a feedback EPSP (cyan) and mono-synaptically

connected PN (red, voltage clamp) received an IPSC. Bath applied GABA_A receptor

antagonist (bicuculline) abolished both the feedback EPSP in the IN and the monosynaptic

IPSC in the PN (black traces). Inset: enlarged trace of IN evoked feedback-EPSP and block

by bicuculline. **(B, C)** Recording from different IN - PN pair showing feedforward

connection. **(B)** Upper two traces, the IN (blue) was voltage clamped (-70 mV) and a

depolarising voltage step (70 mV, 0.5 ms) evokes a feedback EPSC in 39 of 47 trials. Note

that there is no response in the PN (current clamp; resting V_m -55 mV), demonstrating

absence of direct monosynaptic connection. Lower traces from the same pair show an evoked

feedback burst EPSC (8/47 trials). With the feedback burst the PN receives a delayed

summating inhibition **(C)** The delayed IPSP in the PN reverses polarity near -60 mV. **(D)** Plot

illustrates distribution of onset latency of the delayed polysynaptic IPSPs in PNs (n=8 pairs,

72 trials, 1 ms bins).

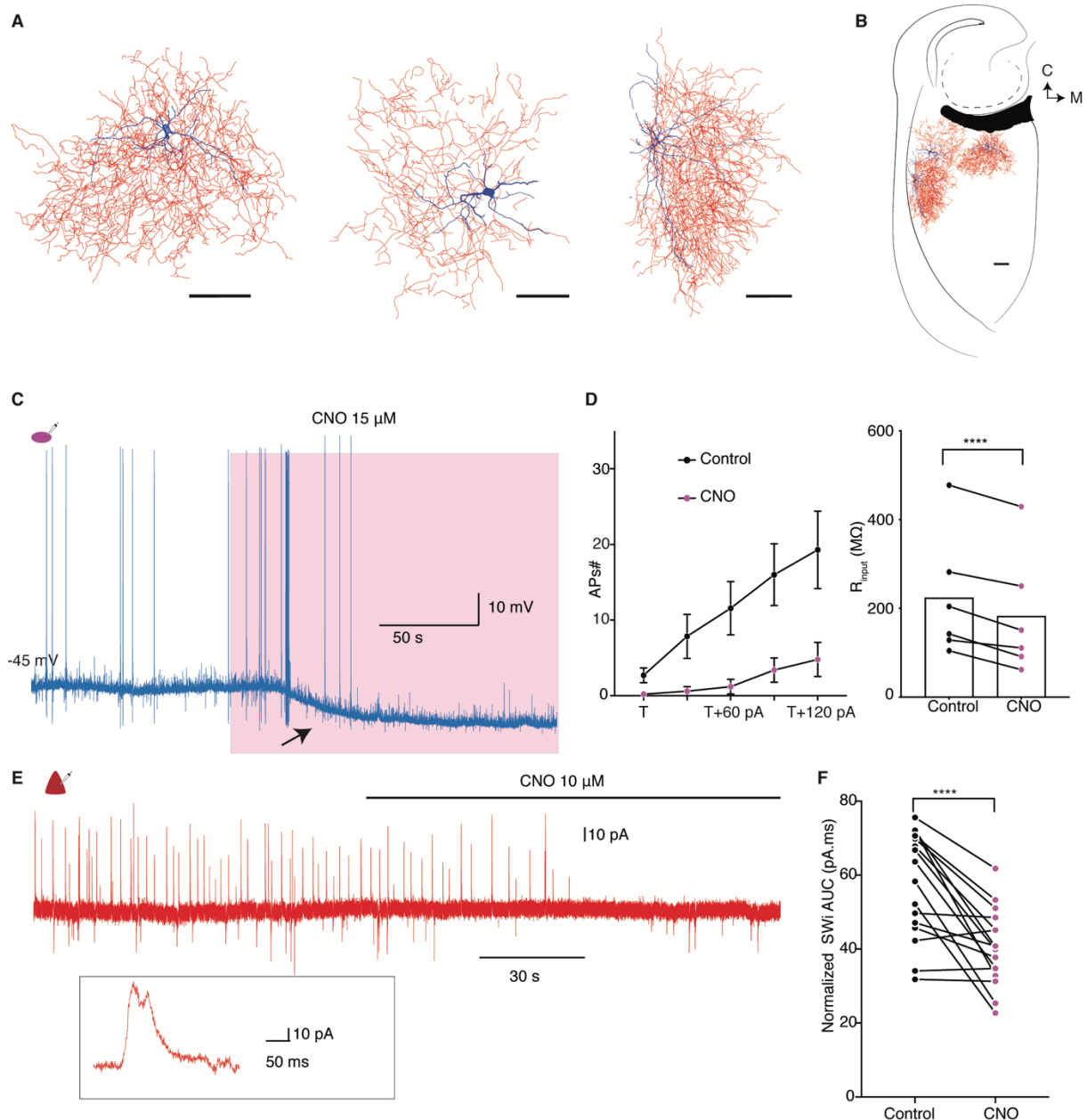


Figure S5. Chandelier interneurons densely innervate the basolateral amygdala and are required to generate sharp wave burst. Related to Figure 3.

(A) Digital reconstructions of three parvalbumin (PV) expressing chandelier INs recovered after staining for biocytin. Somata and dendrites are marked in blue and axons in red. Cell on top left also shown in figure 3B. Scale bar: 100 μm . (B) The schematic shows their location and extent of innervation in the basolateral amygdala (BLA). Scale bar: 100 μm . (C-F) Silencing of PV INs reduces SW-burst. Using PV-Cre mice, a CNO activated inhibitory DREADD hMDGi was expressed in PV-INs in the BLA. (C) Current clamp recording from a PV IN expressing DREADDi depolarized with current injection. Exposure to CNO (pink box) hyperpolarized membrane potential (arrow) and reduced spontaneous action potential discharge. (D) Plotted are the number of action potentials evoked by a 600ms current injection, application of CNO significantly reduced AP discharge. 'T' – threshold current step to elicit first action potential discharge in control. Plot on the right shows the change in input resistance in the presence of CNO in the same cells ($n=7$, $224 \pm 140 \text{ MOhm}$ vs $183 \pm 137 \text{ MOhm}$, paired t-test, $P = 0.0008$). (E) Voltage clamp recording ($V_h = -50\text{mV}$) in a PN in a slice expressing hMDGi. Spontaneous, burst of summing IPSCs (shown in inset) mark the occurrence of SWs.

Application of CNO reduced SWs. **(F)** Plot showing reduction in the amplitude of SW-IPSCs (n=7 cells/slices) and SW-EPSCs (n=7 cells/slices) in the presence of CNO (***) paired t-test, P = 0.0002).

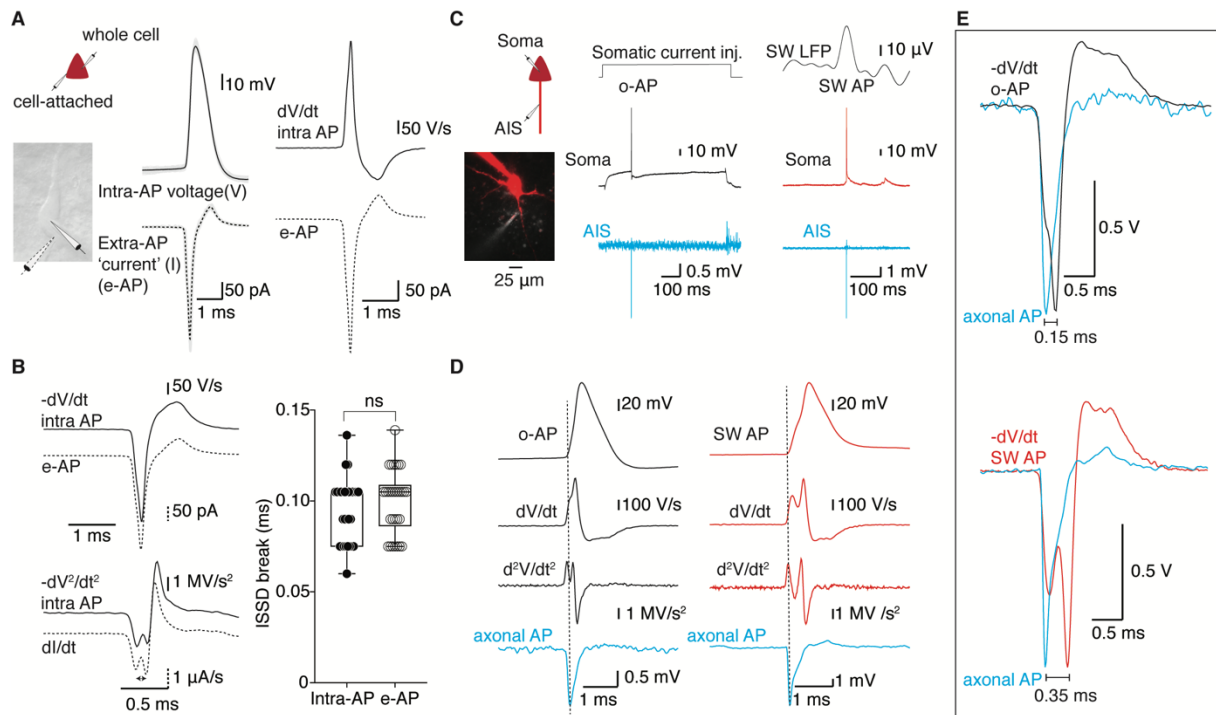


Figure S6. Antidromic action potential in principal neurons during sharp waves. Related to Figure 4.

(A, B) Extracellularly recorded action potential recapitulates the intracellular one. Schematic and photograph show the recording configuration. A whole-cell recording is obtained from the soma of a principal neuron and a second cell-attached extracellular patch pipette placed on the soma. An action potential (intra-AP) is evoked by somatic current injection (left upper trace), and simultaneously seen in the extracellular recording (Extra-AP, lower trace). The first order time-derivative of the intra-AP (upper trace right) has the same time course as the extracellular recorded AP (e-AP, lower trace on right). **(B)** Upper two traces show superimposed inverted first-order time-derivative of intra-AP (solid line) and e-AP (dotted); The second order derivative is shown in the lower two traces, showing two peaks corresponding to the initial segment (IS) and somto-dendritic (SD) components of the AP. The IS-SD break is indicated by the arrow. Right panel shows IS-SD break measured in intra-APs and e-APs ($n=3$ cells, KS test, $P = 0.9$). **(C-D)** Dual patch recording from soma and axon show that action potentials during SW are first seen in the axon then propagate into the soma. **(C)** Schematic and photograph show the recording configuration. A whole-cell intracellular recording was obtained from a PN soma using a pipette containing Alexa 594 (red). A second, loose patch recording was obtained from the axon using a pipette containing Alexa 488 (grey). Traces on the left show the response to somatic current injection (top) that evoked an orthodromic AP (o-AP, black, middle trace, $n=3$), and simultaneously detected at the axon initial segment (AIS, cyan). Traces on the right, show a SW recorded in the local field potential (LFP, top), and the PN discharge ($n=2$) recorded intracellularly (middle, red), and at the AIS (bottom, red). **(D)** Left, top three traces show the o-AP, its first (dV/dt) and the second (d^2V/dt^2) order time-derivative, and the corresponding axonal AP (bottom). The axonal AP aligns with the IS component in the o-AP (dotted line). Right, top three traces show the SW-AP, its first (dV/dt) and the second (d^2V/dt^2) order time derivative, and the corresponding axonal AP (bottom). The axonal AP aligns with the IS component in the SW-AP. **(E)** Top, superimposed traces of normalized inverted dV/dt of the o-AP and the axonal AP illustrating IS-SD break (bidirectional line); bottom, superimposed traces of normalized and inverted dV/dt of the SW-AP (red) and the axonal AP (black), illustrating wider latency between the axonal AP and the somatic components in the SW-AP.

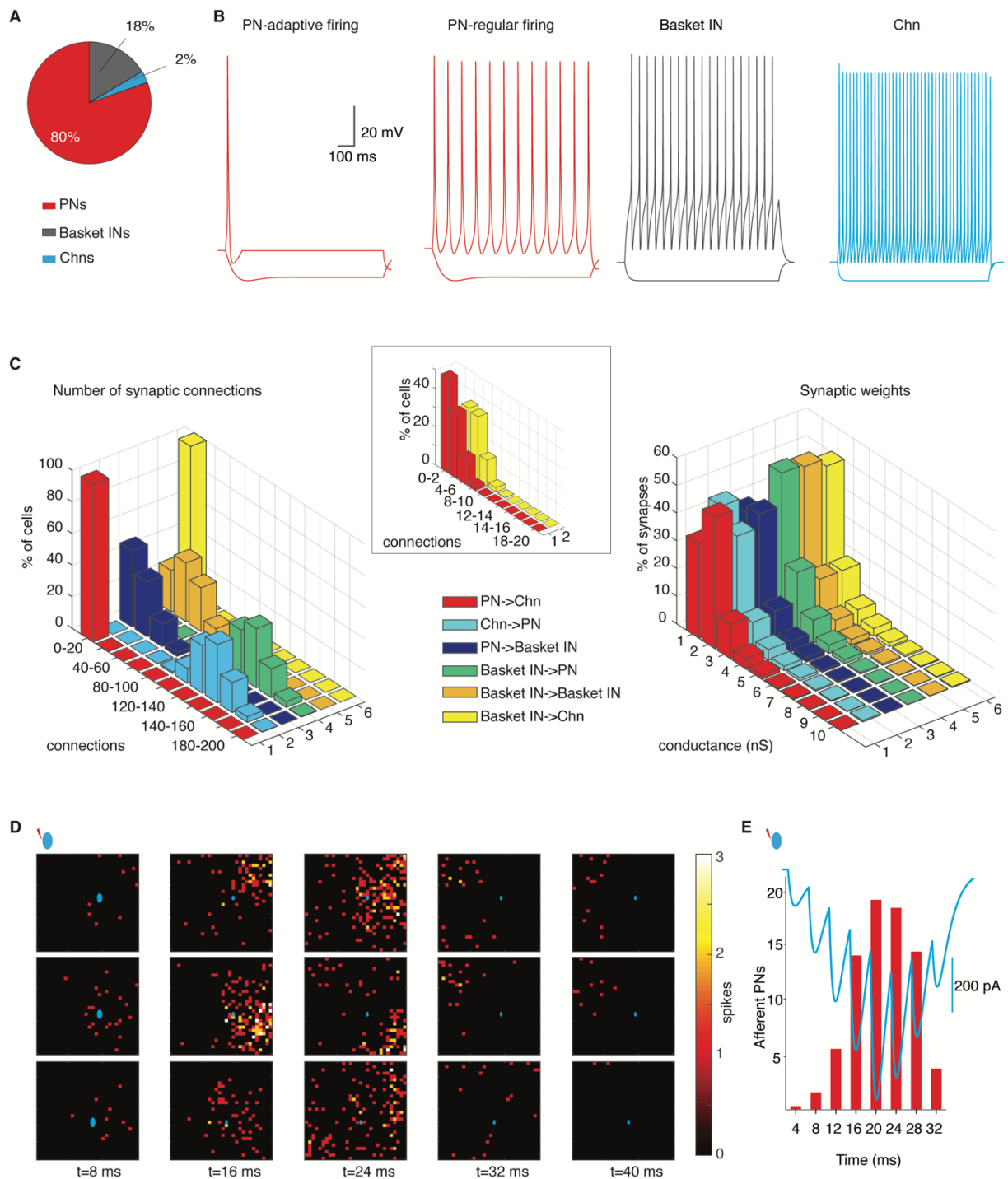


Figure S7 Cellular and synaptic properties of the biophysical network model and generation of sharp wave-associated glutamatergic burst. Related to Figure 7. (A) Cellular composition of network model of the basolateral amygdala comprising of PNs, basket INs and chandelier INs (Chns). (B) Traces of action potential discharge patterns elicited by depolarizing current injection into a biophysical PNs (red), a basket IN (blue) and a Chn (cyan). (C) Left and right, synaptic connections between pairs of cell types and log normal distribution of synaptic strengths in the network model. (D) Chandelier INs (Chns) that evoked sharp waves in each trial recruited different ensembles of PNs. Top to bottom, heat map shows 3 trials of SWs initiated by 3 different Chns; PNs recruited to discharge in

(bright spots) in each trial shows different spatial spread. **(E)** Distribution of synaptic connections underlie summation window of SW EPSC burst. Trace of an evoked SW-burst of EPSCs (cyan) in the network model superimposed with number of afferent PNs (red bars) with spike predicted by the analytical model (see methods). Peak amplitude of SW-EPSCs matches with maximum number of afferent PNs with spikes predicted by the analytical model.

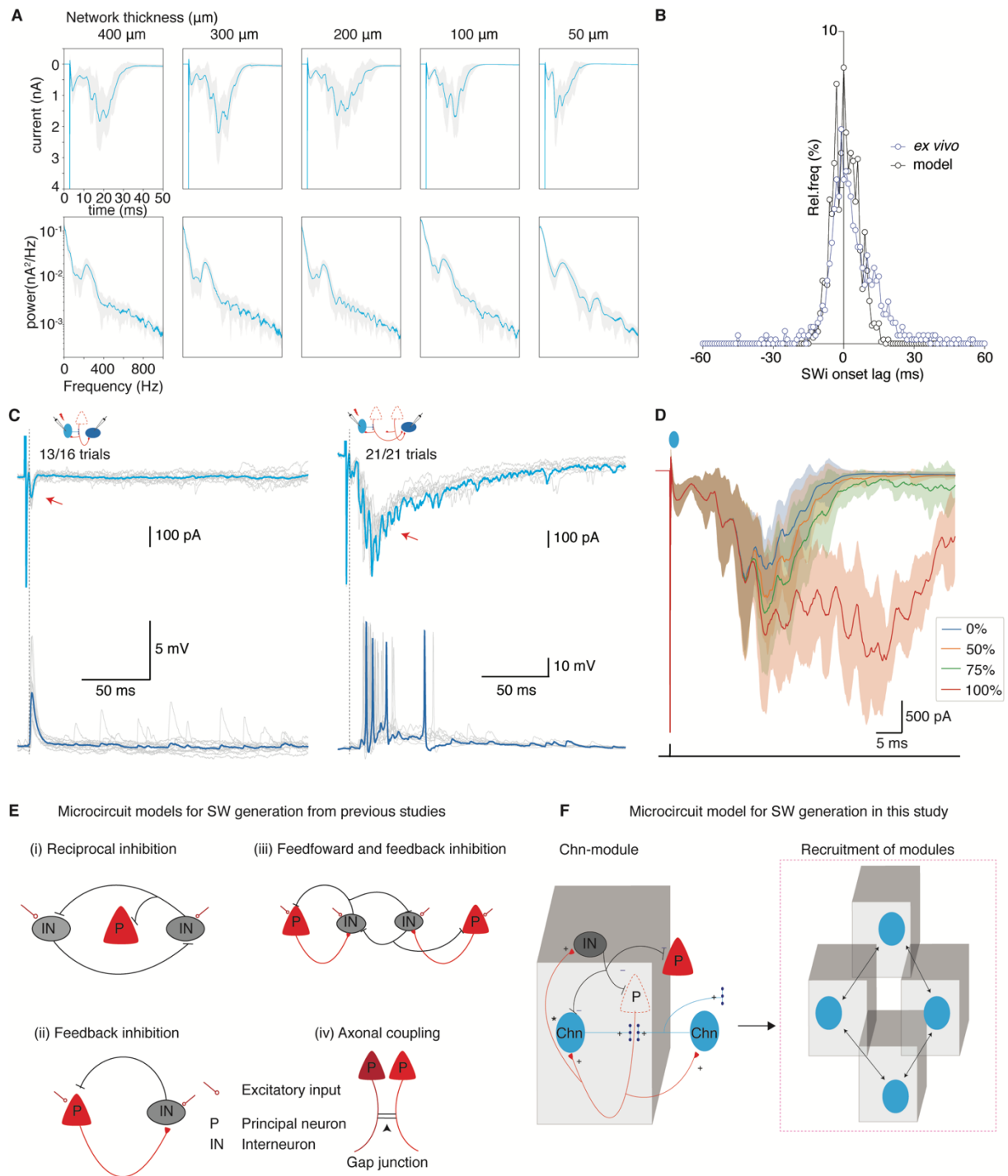


Figure S8. Chandelier IN driven modules reproduce resilience of SW generation, temporal lag and feedforward circuits as in *ex vivo*, and predicts role for basket interneurons – comparison to previous circuit models for SWs (see discussion). Related to Figure 7.

(A) Temporal profile of Chns evoked SW burst of inputs in the model was resilient to loss of circuits. Top and bottom, mean (blue) overlaid on trial-to-trial variation for Chns evoked SW bursts of inputs ($n=16$ cells) and corresponding power spectrum of the evoked burst of inputs. From left to right, the network size was sequentially reduced but Chn initiated SW burst of inputs retained peak frequency at ~ 250 Hz. However, reduction of the network size below 200 μm reduced amplitude and number of feedback cycles in the burst. (B) Histogram shows similar distribution of onset lag of SW-PSPs between pairs of neurons during SWs in the

model (n=1532 values) and in slices (n=24 pairs/742 episodes). **(C)** Model predicted a chandelier IN discharge recruited INs with feedforward excitation (figure 7E) verified by experimental data. Paired recording from a pre-Chn and a post IN. Left, top trace from a Chn shows a single action potential current followed by di-synaptic feedback EPSC, and postsynaptic IN shows time-locked feedforward EPSP. Right, trials when pre-synaptic chandelier IN discharge evoked feedback SW burst inputs, post IN received time-locked SW feedforward burst excitation to driving action potential discharge (n=2 pairs). **(D)** Simulations in the model predict basket-INs activity crucial for the termination of SWs. Results of 16 simulations each with 0, 50, 75, and 100% of Basket INs silenced. Dark traces are the mean of the voltage clamp current on the initiating Chns, the opaque fill represents mean \pm SD (n=16 Chns/trials). **(E)** Previous microcircuit models proposed for generation of SWs in the CA1 hippocampus. **(F)** Chandelier IN (Chn) driven modular microcircuit model for SW generation developed in this study. Note that the chandelier IN driven modules varies in both cellular composition and microcircuit structure from previous models. Unlike models in Ai-iii, chandelier IN driven modules generated SWs solely through intrinsic circuits.